M&C 2017 - International Conference on Mathematics & Computational Methods Applied to Nuclear Science & Engineering, Jeju, Korea, April 16-20, 2017, on USB (2017)

Adjoint-Based Sensitivities for Optimization of Satellite Electron/Proton Shields

Shawn D. Pautz, Brian C. Franke, Brian M. Adams, Laura P. Swiler and Ethan L. Blansett

Sandia National Laboratories, MS 1179, Albuquerque, NM, 87185, sdpautz@sandia.gov

Abstract – *The design of satellites usually includes the objective of minimizing mass due to high launch costs, which is complicated by the need to protect sensitive electronics from the space radiation environment. There is growing interest in automated design optimization techniques to help achieve that objective. Traditional optimization approaches that rely exclusively on response functions can be quite expensive when applied to transport problems. Gradient-based optimization algorithms can also be expensive if they rely on finite difference calculations to determine response sensitivities. In this paper we derive sensitivities of key satellite performance metrics to some relevant design parameters by means of adjoint techniques that significantly reduce the computational requirements. We apply these techniques to the problem of radiation shielding for satellites and demonstrate their improved performance, particularly as the number of design parameters increases.*

I. INTRODUCTION

Satellites in orbit around Earth encounter harsh radiation environments due to trapped electrons and/or protons. Electronics and other components often require shielding; the amount needed depends on the orbit and the solar cycle. The mass of shielding adds to launch costs and/or subtracts from satellite capabilities, so there is motivation to optimize the shielding in order to minimize the mass. If multiple shielding materials are under consideration, the optimal design is not obvious due to competing physical processes [1].

Recently there has been a growing body of work in the radiation transport community on the use of adjoint problems to inexpensively obtain sensitivities of output quantities of interest to various input parameters [2,3]. These sensitivities can be used directly, or through an intermediate response surface, to answer various analysis questions. This adjoint-based approach has been used primarily to inform uncertainty quantification (UQ) studies.

In the present work we will apply the above techniques to the problem of satellite shielding design optimization. We will derive expressions for the sensitivities of dose to electronics with respect to parameters relevant to such designs. We will then incorporate these sensitivities into an optimization algorithm and apply that algorithm to some representative satellite shielding problems.

II. DESCRIPTION OF THE ACTUAL WORK

1. Previous Work

We begin by briefly reviewing previous work that derived a general expression for sensitivities [3]. The general problem to be considered is

$$\Omega \cdot \nabla\psi + \sigma_t(r,E)\psi = \int_{E'} dE' \int_{4\pi} d\Omega' \sigma_s(r,\Omega' \to \Omega, E' \to E)\psi(r,\Omega',E') + q \tag{1a}$$

$$\psi = \psi_b(r,\Omega,E), \{r \in \partial D | \Omega \cdot \vec{n} < 0\} \tag{1b}$$

$$R = \int_D dr \int_E dE \int_{4\pi} d\Omega \psi(r,\Omega,E) q^\dagger(r,E) \tag{1c}$$

Equation (1a) is the familiar Boltzmann transport equation with boundary conditions given by Eq. (1b) and response given by Eq. (1c). In the case of satellite shielding one important response is dose to a component with $q^\dagger = \sigma_d(r,E)/V$.

For simplicity of notation we may express Eq. (1a) as

$$L\psi + C\psi = S\psi + q \tag{2}$$

We also define a general inner product

$$\int_D dr \int_E dE \int_{4\pi} d\Omega ab \equiv \langle a,b \rangle \tag{3}$$

We introduce a Lagrangian and its derivative with respect to a general input parameter *p*:

$$\mathcal{L} = \langle \psi, q^\dagger \rangle - \langle \psi^\dagger, L\psi + C\psi - S\psi - q \rangle \tag{4a}$$

$$\frac{d\mathcal{L}}{dp} = \frac{\partial \mathcal{L}}{\partial p} + \frac{\partial \mathcal{L}}{\partial \psi}\frac{\partial \psi}{\partial p} \tag{4b}$$

After combining Eqs. (2)-(4) and performing various manipulations it can be shown that

$$\frac{d\mathcal{L}}{dp} = \left[\left\langle \psi, \frac{\partial q^\dagger}{\partial p}\right\rangle + \left\langle \psi^\dagger, \frac{\partial q}{\partial p}\right\rangle - \left\langle \psi^\dagger, \left(\frac{\partial}{\partial p}(L + C - S)\right)\psi\right\rangle + \left\langle \frac{\partial \psi}{\partial p}, q^\dagger - \left(L^\dagger + C^\dagger - S^\dagger\right)\psi^\dagger\right\rangle + \left\langle \frac{\partial \psi^\dagger}{\partial p}, q - (L + C - S)\psi\right\rangle\right] + \left[\left\langle I, q^\dagger - \left(L^\dagger + C^\dagger - S^\dagger\right)\psi^\dagger\right\rangle + \left\langle \frac{\partial \psi^\dagger}{\partial \psi}, q - (L + C - S)\psi\right\rangle\right]\frac{\partial \psi}{\partial p} \tag{5}$$

If we impose the condition that ψ and $\psi^\dagger$ satisfy the following forward and adjoint problems:

$$(L + C - S)\psi = q \tag{6a}$$

$$(L^\dagger + C^\dagger - S^\dagger)\psi^\dagger = q^\dagger \tag{6b}$$

then Eq. (5) reduces to

$$\frac{d\mathcal{L}}{dp} = \left[\left\langle \psi, \frac{\partial q^\dagger}{\partial p}\right\rangle + \left\langle \psi^\dagger, \frac{\partial q}{\partial p}\right\rangle - \left\langle \psi^\dagger, \left(\frac{\partial}{\partial p}(L + C - S)\right)\psi\right\rangle\right] = \frac{dR}{dp} \tag{7}$$

Eq. (7) indicates that the sensitivity of a response *R* to a parameter *p* is given by inner products involving a forward solution ψ, an adjoint solution $\psi^\dagger$, and derivatives of transport operators and sources; no other output quantities or derivatives are needed. The same ψ and $\psi^\dagger$ are needed for any arbitrary *p*; only the inner product varies for different parameters. Thus two transport solves in conjunction with numerous relatively inexpensive inner products may be used to obtain any number of sensitivities. This reduction in the number of transport calculations (relative to finite difference techniques) is the key to potential improved algorithmic performance.

2. Application to Satellite Shield Design

A. General Considerations

The mass optimization of satellite shielding for combined electron/proton environments is a complicated problem due to several competing phenomena [1]. For electrons the following processes are important:

- Inelastic scattering (which contributes to shield effectiveness) is proportional to Z/A
- Elastic scattering (which contributes to shield effectiveness) is proportional to Z^2/A
- Production of bremsstrahlung (which degrades shield effectiveness) is proportional to Z^2/A
- Absorption of bremsstrahlung (which contributes to shield effectiveness) generally improves with higher Z, but it depends on the particular electronic shell structure

For protons the dominant effect is inelastic scattering, which is proportional to Z/A. (In this work we will neglect the production of secondary particles due to nuclear interactions.) The balancing of the above effects is non-obvious and thus could benefit from automated optimization techniques.

In order to apply the results of the previous section to satellite shield designs we need to specialize Eq. (7) for parameters of interest for that problem. For simplicity we assume one-dimensional slab geometry, that the shield consists of one or more discrete layers, and that each layer consists of a homogeneous mixture or superposition of an arbitrary combination of candidate materials. The design parameters for a fixed number of layers are the thickness of each layer and the volume fraction of each candidate material in each layer.

B. Sensitivity to Material Fractions

In order to derive the sensitivities of the response to the material volume fractions we first rewrite *C* and *S* to explicitly show the dependence on material fractions p_m for the multigroup approximation:

$$C\psi = \sum_m p_m(\sigma_{t,g,m} - \sigma_{\delta,gg,m})\psi_g \tag{8a}$$

$$S\psi = \sum_{g'}\sum_m p_m M(\Sigma_{g'g,m} - \delta_{g'g}\sigma_{\delta,g'g,m}I)D\psi_{g'} \tag{8b}$$

where we have explicitly incorporated the extended transport correction, which is often used to improve the accuracy of charged-particle calculations. We note that *L* and *q* do not depend on material composition choices, which we also assume is true for $q^\dagger$ for this problem (i.e. we are not free to change the design of a sensitive electronic component).

The corresponding derivatives of *C* and *S* with respect to the material fractions are given by:

$$\frac{\partial C}{\partial p_m} = \sigma_{t,g,m} - \sigma_{\delta,gg,m} \tag{9a}$$

$$\frac{\partial S}{\partial p_m} = \sum_{g'} M(\Sigma_{g'g,m} - \delta_{g'g}\sigma_{\delta,g'g,m}I)D \tag{9b}$$

Substitution of Eqs. (9) into Eq. (7) yields the sensitivity of the response to the volume fraction $p_{m,i}$ of material *m* in region *i*:

$$\frac{dR}{dp_{m,i}} = -\langle\psi_g^\dagger, \left(\frac{\partial C}{\partial p_{m,i}}\right)\psi_{g'}\rangle + \langle\psi_g^\dagger, \left(\frac{\partial S}{\partial p_{m,i}}\right)\psi_{g'}\rangle$$

$$= (\sigma_{\delta,gg,m} - \sigma_{t,g,m})\langle\psi_g^\dagger, \psi_g\rangle_{D_i} + \langle\psi_g^\dagger, \sum_{g'} M(\Sigma_{g'g,m} - \delta_{g'g}\sigma_{\delta,g'g,m}I)D\,\psi_{g'}\rangle_{D_i}$$

$$= \langle\psi_g^\dagger, \sum_{g'} M\Sigma_{g'g,m}D\,\psi_{g'}\rangle_{D_i} + \sigma_{\delta,gg,m}\langle\psi_g^\dagger, (I - MD)\psi_g\rangle_{D_i} - \sigma_{t,g,m}\langle\psi_g^\dagger, \psi_g\rangle_{D_i} \tag{10}$$

We note that the middle term of Eq. (10) is identically zero when *MD=I* (as with continuous transport), but this condition may be violated by angular discretization, particularly for charged-particle transport.

C. Sensitivity to Material Interface Locations

We first rewrite *C*, *S*, and $q^\dagger$ to account for the spatial dependence introduced by transitions from one material region to another at a material interface:

$$C\psi = [H(x-x_{1l}) - H(x-x_i)]\sum_m p_{m,1}\left(\sigma_{t,g,m,1} - \sigma_{\delta,gg,m,1}\right)\psi_g + [H(x-x_i) - H(x-x_{2r})]\sum_m p_{m,2}\left(\sigma_{t,g,m,2} - \sigma_{\delta,gg,m,2}\right)\psi_g \quad (11a)$$

$$S\psi = [H(x-x_{1l}) - H(x-x_i)]\sum_{g'}\sum_m p_{m,1}M\left(\Sigma_{g'g,m,1} - \delta_{g'g}\sigma_{\delta,g'g,m,1}I\right)D\psi_{g'} + [H(x-x_i) - H(x-x_{2r})]\sum_{g'}\sum_m p_{m,2}M\left(\Sigma_{g'g,m,2} - \delta_{g'g}\sigma_{\delta,g'g,m,2}I\right)D\psi_{g'} \quad (11b)$$

$$q^\dagger = [H(x-x_{1l}) - H(x-x_i)]\frac{\sigma_{d,g,1}}{\rho_1 V_1} + [H(x-x_i) - H(x-x_{2r})]\frac{\sigma_{d,g,2}}{\rho_2 V_2} \quad (11c)$$

Here index "1" indicates the region/material to the left of the interface and "2" the region to the right. Although earlier we ignored the effect of material choices on $q^\dagger$, we do here anticipate the effect of spatial placement of a sensitive component, which could become important in multidimensional analysis. We also note that typically either $\sigma_{d,g,1}$ or $\sigma_{d,g,2}$ (but not both) will contribute to a response such as dose; we include both for generality.

The corresponding derivatives of *C*, *S*, and $q^\dagger$ with respect to the material interface location are:

$$\frac{\partial C}{\partial x_i} = \delta(x-x_i)\sum_m p_{m,1}\left(\sigma_{t,g,m,1} - \sigma_{\delta,gg,m,1}\right) - \delta(x-x_i)\sum_m p_{m,2}\left(\sigma_{t,g,m,2} - \sigma_{\delta,gg,m,2}\right) \quad (12a)$$

$$\frac{\partial S}{\partial x_i} = \delta(x-x_i)\sum_{g'}\sum_m p_{m,1}M\left(\Sigma_{g'g,m,1} - \delta_{g'g}\sigma_{\delta,g'g,m,1}I\right)D - \delta(x-x_i)\sum_{g'}\sum_m p_{m,2}M\left(\Sigma_{g'g,m,2} - \delta_{g'g}\sigma_{\delta,g'g,m,2}I\right)D \quad (12b)$$

$$\frac{\partial q^\dagger}{\partial x_i} = \{V_1\delta(x-x_i) - [H(x-x_{1l}) - H(x-x_i)]\}\frac{\sigma_{d,g,1}}{\rho_1 V_1^2} + \{-V_2\delta(x-x_i) + [H(x-x_i) - H(x-x_{2r})]\}\frac{\sigma_{d,g,2}}{\rho_2 V_2^2} \quad (12c)$$

We will consider each of the expressions in Eq. (12) separately. Substitution of Eq. (12a) into Eq. (7) yields

$$\begin{aligned}\frac{dR}{dx_i} &= -\langle\psi_g^\dagger, \left(\frac{\partial C}{\partial x_i}\right)\psi_{g'}\rangle \\ &= -\langle\psi_g^\dagger, \delta(x-x_i)\sum_m p_{m,1}\left(\sigma_{t,g,m,1} - \sigma_{\delta,gg,m,1}\right)\psi_g\rangle \\ &\quad + \langle\psi_g^\dagger, \delta(x-x_i)\sum_m p_{m,2}\left(\sigma_{t,g,m,2} - \sigma_{\delta,gg,m,2}\right)\psi_g\rangle \\ &= -\sum_g \int_{4\pi} d\Omega\psi_g^\dagger(x_i,\Omega)\sum_m p_{m,1}\left(\sigma_{t,g,m,1} - \sigma_{\delta,gg,m,1}\right)\psi_g(x_i,\Omega) \\ &\quad + \sum_g \int_{4\pi} d\Omega\psi_g^\dagger(x_i,\Omega)\sum_m p_{m,2}\left(\sigma_{t,g,m,2} - \sigma_{\delta,gg,m,2}\right)\psi_g(x_i,\Omega) \\ &= \sum_g\sum_m p_{m,2}\left(\sigma_{t,g,m,2} - \sigma_{\delta,gg,m,2}\right)\int_{4\pi} d\Omega\psi_g^\dagger(x_i,\Omega)\psi_g(x_i,\Omega) \\ &\quad - \sum_g\sum_m p_{m,1}\left(\sigma_{t,g,m,1} - \sigma_{\delta,gg,m,1}\right)\int_{4\pi} d\Omega\psi_g^\dagger(x_i,\Omega)\psi_g(x_i,\Omega)\end{aligned} \quad (13)$$

Substitution of Eq. (12b) into Eq. (7) yields

$$\begin{aligned}\frac{dR}{dx_i} &= \langle\psi_g^\dagger, \left(\frac{\partial S}{\partial x_i}\right)\psi_{g'}\rangle \\ &= \langle\psi_g^\dagger, \delta(x-x_i)\sum_{g'}\sum_m p_{m,1}M\left(\Sigma_{g'g,m,1} - \delta_{g'g}\sigma_{\delta,g'g,m,1}I\right)D\,\psi_{g'}\rangle \\ &\quad - \langle\psi_g^\dagger, \delta(x-x_i)\sum_{g'}\sum_m p_{m,2}M\left(\Sigma_{g'g,m,2} - \delta_{g'g}\sigma_{\delta,g'g,m,2}I\right)D\,\psi_{g'}\rangle \\ &= \sum_g\int_{4\pi} d\Omega\psi_g^\dagger(x_i,\Omega)\sum_{g'}\sum_m p_{m,1}M\left(\Sigma_{g'g,m,1} - \delta_{g'g}\sigma_{\delta,g'g,m,1}I\right)D\,\psi_{g'}(x_i,\Omega) \\ &\quad - \sum_g\int_{4\pi} d\Omega\psi_g^\dagger(x_i,\Omega)\sum_{g'}\sum_m p_{m,2}M\left(\Sigma_{g'g,m,2} - \delta_{g'g}\sigma_{\delta,g'g,m,2}I\right)D\,\psi_{g'}(x_i,\Omega)\end{aligned} \quad (14)$$

Substitution of Eq. (12c) into Eq. (7) yields

$$\frac{dR}{dx_i} = \langle \psi_g, \frac{\partial q^\dagger}{\partial x_i} \rangle$$
$$= \langle \psi_g, \{V_1 \delta(x - x_i) - [H(x - x_{1l}) - H(x - x_i)]\} \frac{\sigma_{d,g,1}}{\rho_1 V_1^2} \rangle$$
$$+ \langle \psi_g, \{-V_2 \delta(x - x_i) + [H(x - x_i) - H(x - x_{2r})]\} \frac{\sigma_{d,g,2}}{\rho_2 V_2^2} \rangle$$
$$= \frac{1}{\rho_1 V_1} \sum_g \sigma_{d,g,1} \int_{4\pi} d\Omega \psi_g(x_i, \Omega) - \frac{1}{\rho_1 V_1^2} \sum_g \sigma_{d,g,1} \int_{4\pi} d\Omega \int_{D1} dr \psi_g(r, \Omega)$$
$$- \frac{1}{\rho_2 V_2} \sum_g \sigma_{d,g,2} \int_{4\pi} d\Omega \psi_g(x_i, \Omega) + \frac{1}{\rho_2 V_2^2} \sum_g \sigma_{d,g,2} \int_{4\pi} d\Omega \int_{D2} dr \psi_g(r, \Omega) \quad (15)$$

Summation of Eqs. (13)-(15) yields the overall sensitivity of the response to changes in the location of a material interface. Alternatively, the sensitivity to the thickness of one of the regions may be obtained by neglecting the terms in Eqs. (13)-(15) associated with the region on the opposite side of the interface.

D. Incorporation of Sensitivities in Design Optimization

Solution of Eqs. (6a) and (1c) provides the response for a particular design configuration and is the basic computational kernel for simple but potentially expensive optimization algorithms. Solution of Eqs. (6b), (10), and (13)-(15) provides the gradients of the response and, in conjunction with the results of Eqs. (6a) and (1c), is the basic computational kernel for more complicated but potentially more efficient optimization algorithms. In the present work we use the SCEPTRE deterministic radiation transport code [4] and associated postprocessing tools to solve Eqs. (1) and (6). We have created new postprocessing tools to solve Eqs. (10) and (13)-(15). Finally, we link Dakota [5] and its included NPSOL local, gradient-based optimization library [6] to the above computational kernels to drive our design optimization process.

We note that we have identified two different problem formulations that are equivalent in slab geometry for the continuous equations. In "thickness" studies we use Eqs. (10) and (13)-(15) to vary both the thickness and composition of each region, and we constrain the material volume fractions to sum to unity. In "density" studies we use only Eq. (10) by fixing the thickness of each region to arbitrary nominal values and by allowing the sum of the material fractions to be unconstrained, i.e. the densities chosen may not be physically realistic. We may scale the densities and thicknesses afterwards to achieve nominal densities. We use these two formulations to explore the behavior of constrained versus unconstrained optimization and also the particular characteristics of Eqs. (10) and (13)-(15).

To be more precise, our constrained optimization problem can be expressed as

Thickness formulation

$$\begin{aligned} &min_{t,p} mass(t,p) \\ &s.t. dose(t,p) \leq 10\ krad \\ &\sum p_m = 1 \\ &0 \leq t \leq t_{max} \\ &0 \leq p_m \leq 1 \end{aligned} \quad (16a)$$

Density formulation

$$\begin{aligned} &min_p mass(p) \\ &s.t. dose(p) \leq 10\ krad \\ &0 \leq p_m \end{aligned} \quad (16b)$$

Our assumption that materials may be arbitrarily mixed may not be practical from an engineering standpoint. But it does result in a simpler, more tractable, continuous optimization problem; only the number of layers is a discrete quantity. If materials may not be mixed in this manner (e.g. if only single materials like aluminum or steel are allowed in any particular region due to manufacturing realities) we then have a discrete optimization problem, which is more difficult and costly to solve. We have not yet addressed discrete decision variables.

III. RESULTS

A. Problem Definition and Setup

The problem we wish to study is depicted in Figure 1. We assume that a satellite has a 0.762 mm (30 mil) layer of aluminum as structural material (we discuss later an issue that can arise without such a fixed outer layer). Inside of that is a small silicon component coated with epoxy. In between we wish to place one or more shielding layers of thickness and composition to be determined by our optimization tools. Isotropic radiation is incident on the left with vacuum boundary conditions on the right. We have studied various candidate materials: in some cases, we allowed only ultra-high molecular weight polyethylene (UHMWPE), in other cases we have allowed for a few typical metals of low, medium, and high Z, and in yet other cases we have allowed for any elements in the periodic table up to and including uranium. While shields comprised of these materials may not be manufacturable, the resulting optimal designs indicate what is theoretically possible and may inspire novel processes for shield manufacturing. The satellite is placed in a circular equatorial orbit at several altitudes; much of our focus will be at 3000 km altitude [1]. We impose the requirement of limiting dose to 10 krad/year due to trapped electrons and protons.

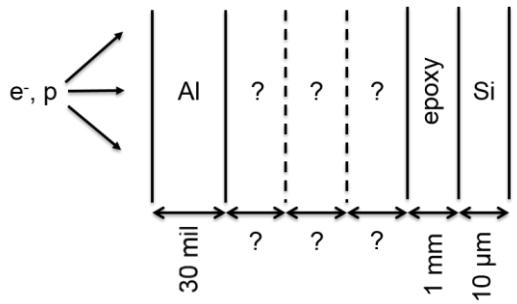

Fig. 1. Diagram of satellite shielding problem (not to scale).

For boundary conditions we use the AE8 and AP8 models in Spenvis [7] to define the radiation environment. For material properties we use CEPXS [8] to generate electron/photon/positron cross sections with P_{13} scattering and LITXS [9] to generate proton cross sections. LITXS assumes that protons are only slowed down without angular deflection or secondary production. All transport calculations are solved in SCEPTRE to within 10^{-4} iterative tolerance on a spatial mesh of comparable error for dose calculations. For the Dakota optimization process, we use a convergence tolerance and a constraint tolerance of 10^{-3}. We also make use of logarithmic scaling of the dose. As an initial design point we use either all UHMWPE (when only a few materials are available) or equal volume fractions of all materials (when most/all of the periodic table is considered).

B. Optimization Results

We conducted a large series of design studies in which we compared the performance of our adjoint-based optimization algorithm to one based on forward finite difference derivatives. In the finite difference (FD) approach sensitivities are estimated by making a small perturbation to each design parameter in turn, running a forward transport and response calculation, and differencing with the nominal response. Thus the FD approach requires P+1 transport solves at each point in the design space, where P is the number of optimization parameters. We summarize some of the results in Table I. The first four columns list the problem characteristics: the number of layers, the candidate materials, whether the density or thickness problem formulation was used, and the resulting number of design parameters in the problem. The fifth column lists the number of iterations required for convergence by our algorithm (forward + adjoint: "F+A") and by the finite difference approach ("FD"). An iteration consists of the evaluation of the response for a set of design parameter values chosen by the optimization algorithm and any other calculations needed to obtain sensitivities. Since both algorithms rely on the same underlying optimization algorithm any differences in the number of iterations occur due to differences in the sensitivity estimates. The last column lists the total number of transport solves (either forward or adjoint) required by both algorithms; the total computational cost scales according to that number. In some cases, there are no results for the FD approach because it was too expensive to run to completion.

These results show that both algorithms behave approximately the same in terms of number of iterations. They also converge to generally the same design (which we do not report here). For a small number of design parameters, the computational cost may be similar, but as the number of design parameters increases the finite difference approach can become cost-prohibitive since it scales linearly with the number of parameters.

In order to illustrate the design process itself we examine more closely the sixth problem italicized in Table I. This problem consists of five potential materials in one layer and uses the thickness formulation for design. In Table II we report the thickness, the material fractions, the total mass, and the dose at each design iteration. Note that the NPSOL optimization algorithm does not necessarily converge monotonically to the final design point, as it is working to reduce mass while simultaneously striving to satisfy the nonlinear (and implicit through the simulation) dose constraint. During iteration, some designs have lower mass, but are infeasible with respect to the dose constraint. Eventually it completes when it determines that it has minimized the objective and satisfied the constraints to within the desired tolerance.

The final design point should be at least a local minimum. At that point all sensitivities should be of identical magnitude, with the exception of smaller magnitudes for materials that were eliminated (i.e. have zero volume fractions). In order to demonstrate that our algorithm achieves this we examine the parameter sensitivities of the final design from the process shown in Table II. These sensitivities are reported in Table III. Here we note that the sensitivities of the thickness and of the materials with non-zero fractions are approximately the same, whereas the sensitivities of materials not selected are of smaller magnitude. This is consistent with other studies we have performed. Although in this case the sensitivity for tantalum is somewhat lower in magnitude than those for thickness or UHMWPE, we note that its volume fraction is within the desired tolerance so the algorithm is free to terminate.

Table I. Comparison of adjoint- and finite-difference-based optimization algorithmic behavior for 3000 km orbit.

layers	candidate materials	formulation	P	F+A/FD iterations	F+A/FD solves
1	UHMWPE	density	1	4/4	8/8
1	UHMWPE	thickness	1	2/2	4/4
1	UHMWPE, Al	density	2	11/11	22/33
1	UHMWPE, Al	thickness	3	5/5	10/20
1	UHMWPE, Al, Cu, Mo, Ta	density	5	22/14	44/84
1	*UHMWPE, Al, Cu, Mo, Ta*	*thickness*	*6*	*17/19*	*34/133*
2	UHMWPE, Al, Cu, Mo, Ta	thickness	12	30/29	60/377
1	periodic table	density	92	13/-	26/-
2	periodic table	density	184	15/-	30/-

Table II. Optimization design process behavior for the one-layer thickness optimization formulation italicized in Table I.

iteration	thickness (cm)	UHMWPE fraction	Al fraction	Cu fraction	Mo fraction	Ta fraction	mass (g/cm^2)	dose (krad)
1	13.50	1.0000	0	0	0	0	12.55	10.01
2	12.61	0.9998	0	0	0	0.0002	11.76	10.45
3	4.69	0.9939	0	0	0	0.0061	4.81	27.46
4	10.58	1.0000	0	0	0	0	9.83	13.90
5	8.38	0.9977	0	0	0	0.0023	8.09	16.28
6	4.87	0.9940	0	0	0	0.0060	4.98	26.62
7	10.71	1.0000	0	0	0	0	9.96	13.68
8	8.69	0.9979	0	0	0	0.0021	8.36	15.69
9	12.42	1.0000	0	0	0	0	11.55	11.24
10	11.13	0.9993	0	0	0	0.0007	10.47	11.93
11	11.28	0.9904	0	0	0	0.0096	12.18	10.80
12	11.14	0.9990	0	0	0	0.0010	10.53	11.87
13	11.13	0.9992	0	0	0	0.0008	10.48	11.92
14	12.74	0.9995	0	0	0	0.0005	11.94	10.09
15	11.64	0.9993	0	0	0	0.0007	10.94	11.29
16	12.78	0.9995	0	0	0	0.0005	11.99	10.04
17	12.81	0.9994	0	0	0	0.0006	12.02	10.00

Table III. Sensitivity of dose to design variables for final design.

Parameter	Sensitivity (krad-cm^2/gm)
Thickness	-1.092
UHMWPE	-1.093
Al	-0.815
Cu	-0.923
Mo	-0.874
Ta	-1.013

To demonstrate how the optimization algorithm adapts to the different physics of different particle types we examine the density variant of the problem reported in Tables II and III. We reran the problem with only electron sources and with only proton sources. Although these separate environments will not occur in nature for the relevant orbit, it does help illustrate the behavior of our algorithm. In Table IV we report the optimized design for each of these environments. Note that both the material selections and mass vary as the particle types vary, and in ways that make physical sense. Also note that the optimized design for the full electron/proton environment is not merely a superposition of the single-particle designs, even though the same materials are involved.

Table IV. Effect of radiation environment particle types on optimal design (g/cm^2)

material	electrons	protons	both
UHMWPE	0	11.92	11.89
Al	0	0	0
Cu	0	0	0
Mo	0	0	0
Ta	0.441	0	0.138

In Table V we compare the behavior of the density and thickness variants of our algorithm and also the effects of allowing multiple layers for the problem of Table IV. Here we see that there is very little difference between the results of the two algorithmic forms, as we expect. Not shown is that the two forms may take different paths to get to the same final design, since the thickness approach has an additional design parameter and an additional constraint. We also see here (and in other studies not depicted) that there is very little improvement by allowing for a heterogeneous shield. Although a multi-layer shield was proposed in [1], we note that we are examining a different set of environments and requirements. We hope to revisit the problem in [1] and/or to identify a set of conditions that would clearly demonstrate the utility and correctness of our algorithm for such designs.

Table V. Resulting optimal shield masses for various design studies (g/cm^2).

layers	algorithm	electrons	protons	both
1	density	0.4411	11.92	12.03
1	thickness	0.4412	11.92	12.03
2	density	0.4411	11.92	12.07
2	thickness	0.4412	11.92	12.05
3	density	0.4415	11.92	---
3	thickness	0.4416	11.92	---

In Table VI we show some additional effects of varying the environment and of varying the set of potential materials. The first column lists the altitude of the orbit (and thus, implicitly, the electron/proton environment). The second column shows the mass of each material for an optimized design when the five materials reported earlier were considered. The third column gives corresponding results when the entire periodic table is considered. This table shows that different materials are selected to shield in each electron/proton environment. Some of the designs are obviously impractical from a materials manufacturing standpoint, but this efficient optimization approach allows us to explore a large design space that could be computationally prohibitive for other algorithms.

Table VI. Results of adjoint-based satellite single-layer shield optimization for varying environments (altitudes).

Altitude (km)	UHMWPE-Al-Cu-Mo-Ta mass (g/cm^2)	Periodic table mass (g/cm^2)
2000	UHMWPE 7.81, Ta 0.126	H 3.95, Ta 0.098
3000	UHMWPE 11.89, Ta 0.138	H 6.03, Ta 0.125
4000	UHMWPE 6.43, Ta 0.166	H 3.19, other 0.290
5000	UHMWPE 2.65, Ta 0.161	H 1.35, Ta 0.131
6000	UHMWPE 1.22, Ta 0.123	H 0.614, Ta 0.109, Pa trace
7000	UHMWPE 0.697, Ta 0.094	H 0.359, Ta 0.075, Pa trace
8000	UHMWPE 0.404, Ta 0.078	H 0.216, Ta 0.056
9000	UHMWPE 0.244, Ta 0.083	H 0.149, At 0.047, Pa trace

C. Algorithmic Issues

In the above subsection we demonstrated the favorable properties of our adjoint-based optimization algorithm. Here we discuss some issues that will need further attention.

In some cases, we have observed "excessive" iterations in order to converge to a result. That is, it appears that the algorithm has achieved a solution within the desired tolerances but it continues searching for an improved solution. In other cases, it appears that the algorithm terminates too soon; the chosen solution does not satisfy constraints to the desired tolerance. It is not clear whether the issue is with the underlying NPSOL solver per se or whether the information being supplied to it is problematic. For example, transport discretization errors could result in inaccurate response or gradient calculations that cause the Dakota optimization algorithm to take too large or too small a step in parameter space, rather than the ideal step that would simultaneously minimize the objective and best satisfy the constraints.

In Section II.C we derived sensitivities to material interface locations. We indicated there that the sensitivities to region thicknesses can be obtained by neglecting the terms associated with the region on the other side of an interface,

which forms the basis for the thickness formulation of our optimization algorithm. Theoretically it should not matter where in a region the surface integrals are performed (i.e. what x_i is in Eqs. (13)-(15)); increasing the thickness of a region in slab geometry should produce the same transport effect regardless of where material is added in that region. We have observed, however, that in practice our computed sensitivities are not constant throughout a region. In Figure 2 we depict the computed thickness sensitivity of tantalum as a function of position for a problem similar to that in Figure 1 with the exception that we have removed the leading region of aluminum and the epoxy coating. As observed in Figure 2 the computed sensitivity is not a constant but varies throughout the region, especially near the extremities. At the leading edge (i.e. that exposed to the space environment) the computed sensitivities are actually positive, which is clearly nonphysical. We have observed similar behavior in other cases: the thickness sensitivities are relatively flat for interior components but deviate near the extremities of the problem. We believe that in these cases the spatial resolution is insufficient to accurately model the boundary layers produced by the lowest-energy particles, which dominate the space environment and to a lesser extent the adjoint sources. Although accurate modeling of these boundary layers is usually unnecessary for the calculation of downstream effects such as dose due to rapid attenuation of errors, it may be needed in this case since the sensitivity calculation depends on local information. In such cases we have found that optimization is problematic since the underlying sensitivities are incorrect. Conversely, we have not observed such issues when the extremities are fixed, as they are in Figure 1. This remains an open research question.

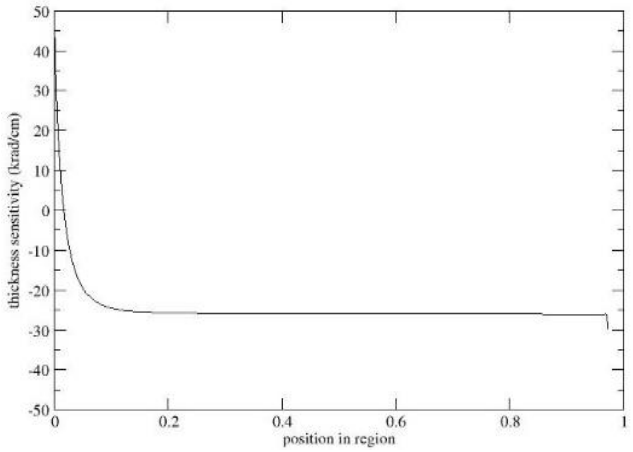

Fig. 2. Computed thickness sensitivity as function of position in region.

IV. CONCLUSIONS

We have demonstrated an initial capability to compute optimized designs for satellite shielding in slab geometry by means of adjoint-based sensitivities. Its computational efficiency should allow for extensive trade studies involving numerous materials and geometric complexity, since it scales well with the number of design parameters. It is hoped that this technique will allow for radiation transport and shielding design to be incorporated efficiently into satellite mechanical design, allowing for optimization and large reductions in satellite mass.

In the future we hope to extend this work to multidimensional calculations. In these geometries the density formulation is not strictly valid; we will need to rely on interface sensitivities. For this reason, we will need to further investigate the causes and corrections to the errors we have observed for such sensitivities. We also need to incorporate multiple objectives, such as when there are components of different sensitivities at different locations. This may require the use of multiple adjoint calculations.

NOMENCLATURE

A = atomic mass number
C = collision operator
D = spatial domain, discrete-to-moment operator
E = particle energy
g = energy group index
i = region index
L = streaming operator
$\mathcal{L}$ = Lagrangian
m = material index
M = moment-to-discrete operator
Ω = particle direction
p = design parameter
$p_{m,i}$ = material volume fraction
ψ = angular flux
$\psi^\dagger$ = adjoint angular flux
q = transport source
$q^\dagger$ = adjoint transport source
r = spatial coordinate
ρ_i = density of region i
R = response to radiation
S = scattering operator
σ_d = dose cross section
σ_s = scattering cross section
σ_t = total cross section
$\Sigma_{g'g,m}$ = multigroup scattering operator
t_i = thickness of region i
V_i = volume of region i
Z = atomic number

ACKNOWLEDGMENTS

Supported by the Laboratory Directed Research and Development program at Sandia National Laboratories, a multi-mission laboratory managed and operated by Sandia Corporation, a wholly owned subsidiary of Lockheed Martin

Corporation, for the U.S. Department of Energy's National Nuclear Security Administration under contract DE-AC04-94AL85000.

REFERENCES

1. W.C. FAN, C.R. DRUMM, S.B. ROESKE, and G.J. SCRIVNER, "Shielding Considerations for Satellite Microelectronics," *IEEE Trans. On Nuclear Science*, **43**, *6*, 2790 (1996).
2. H. F. STRIPLING, M. ANITESCU, and M. L. ADAMS, "A generalized adjoint framework for sensitivity and global error estimation in time-dependent nuclear reactor simulations," *Annals of Nuclear Energy*, **52**, 47 (2013).
3. D.E. BRUSS, *Adjoint-Based Uncertainty Quantification for Neutron Transport Calculations*, Ph.D. Dissertation, Texas A&M University (2016).
4. S. PAUTZ, B. BOHNHOFF, C. DRUMM and W. FAN, "Parallel Discrete Ordinates Methods in the SCEPTRE Project," *Proc. Int. Conf. on Mathematics, Computational Methods and Reactor Physics*, Saratoga Springs, NY, May 3-7, 2009, CD-ROM, American Nuclear Society (2009).
5. B.M. ADAMS, W.J. BOHNHOFF, K.R. DALBEY, J.P. EDDY, M.S. EBEIDA, M.S. ELDRED, P.D. HOUGH, K.T. HU, J.D. JAKEMAN, K.A. MAUPIN, J.A. MONSCHKE, E.M. RIDGWAY, A. RUSHDI, L.P. SWILER, J.A. STEPHENS, D.M. VIGIL, and T.M. WILDEY, "Dakota, A Multilevel Parallel Object-Oriented Framework for Design Optimization, Parameter Estimation, Uncertainty Quantification, and Sensitivity Analysis: Version 6.4 User's Manual," SAND2014-4633, Sandia National Laboratories (2016).
6. P.E. GILL, W. MURRAY, M.A. SAUNDERS, and M.H. WRIGHT, "User's Guide for NPSOL (Version 4.0): A Fortran Package for Nonlinear Programming," TR SOL-86-2, Stanford University (1986).
7. "Space Environment Information System (SPENVIS)", http://www.spenvis.oma.be/spenvis, European Space Agency (2016).
8. L.J. LORENCE, JR., J.E. MOREL, and G.D. VALDEZ, "Physics guide to CEPXS: a multigroup coupled electron-photon cross-section generating code," SAND89-1685, Sandia National Laboratories, Albuquerque, NM (1989).
9. C.R. DRUMM, "Light-Ion Transport Cross Section Code - LITXS," SAND-93-3008, Sandia National Laboratories, Albuquerque, NM (1994).